



Semnan University

# Mechanics of Advanced Composite Structures

journal homepage: <http://MACS.journals.semnan.ac.ir>

## The Effect of Nano-B<sub>4</sub>C Additive on Microstructure and Mechanical Properties of Pressureless Sintering SiC Bodies

B. S. Kozekanan <sup>a</sup>, A. Moradkhani <sup>b\*</sup>, H. Baharvandi <sup>c</sup>, V. Panahizadeh <sup>b</sup>

<sup>a</sup> Department of Mechanical Engineering, University of Tabriz, Tabriz, Iran

<sup>b</sup> Faculty of Mechanical Engineering, Shahid Rajaee Teacher Training University, Tehran, Iran

<sup>c</sup> Department of Materials Engineering, University of Tehran, Tehran, Iran

### KEYWORDS

Mechanical properties;  
Nanocomposite;  
Silicon carbide;  
Nano boron carbide;  
Fracture behavior.

### ABSTRACT

In this study, the mechanical properties, microstructure, and fracture behavior of SiC-NanoB<sub>4</sub>C composites have been investigated with different weight percentages of secondary phase including 0, 0.25, 0.5, 0.75, 1, 2, and 3 wt.% nanoB<sub>4</sub>C produced by pressureless sintering. At least 1 wt.% of phenolic resin was added to all samples as a carbon source (both as a binder and as a carbon additive). Samples were then sintered for 2h at 2150°C under an argon atmosphere. The results showed that the composite containing SiC-0.5wt% nanoB<sub>4</sub>C, sintered at 2150°C, had the best mechanical properties. In this sample, the relative density was 98.32%, the micro-hardness was 28.6 GPa, Young's modulus was 471.8 GPa and the fracture toughness was 3.7 MPa.m<sup>1/2</sup>. Also, the transgranular fracture was observed in the related SEM images. Larger amounts of additives reduced the properties. In order to compare the results better, the temperature and duration of the sintering, the micron-scale size of the B<sub>4</sub>C additive, the amount of phenolic resin, and the amount of initial sample press were considered as variables.

## 1. Introduction

Silicon carbide (SiC) is difficult to be sintered without proper additives due to low permeability and the problem of sintering [1-4]. However, it is highly considered due to its excellent properties such as low density, high thermal conductivity, low thermal expansion coefficient, toughness, and high young's modulus. [1-5]. SiC is attended to due to its high covalent bond volume and suitable mechanical properties used in difficult mechanical conditions [1-3]. It has a 88% covalent bond [2-4], which is the reason for being used as the best option in high temperatures [5]. This high volume of covalent bonding is also a reason for SiC sinter unacceptability or hard acceptability [1-4]. SiC has various applications in different industries such as diesel engine components [6], heat exchangers, high-temperature energy exchange systems [7], hot gas filters [8], car ceramic brakes, fraction discs [9], medical implants [10], optical mirrors [11], and heater and gas turbines [12]. SiC has more than 200 different polytypes. The most famous of

these are 3C, 6H, 2H, and 15R [1, 13-18]. Non-cube transformations are known as  $\alpha$ -SiC, and cubic ones are called  $\beta$ -SiC [1].  $\beta$ -SiC is stable at temperatures below 1800°C [1, 18] while  $\alpha$ -SiC gets stable at higher temperatures. The transformation of  $\beta$  to  $\alpha$  happens through a reaction at a temperature of 1920°C, and this reaction is reversible in the nitrogen atmosphere [1].

Carbon and boron additives can be used for SiC sintering [1-5, 19-21]. Carbon reduces interplanetary energy at the grain boundary, which improves the quality of SiC diffusion in the Argon atmosphere [22]. Boron also increases the diffusion coefficient of C and Si, and this increases the mechanism of sintering [21, 22]. Boron also reduces interface energy by depositing in the grain boundaries which leads to improvement in sintering [21]. In addition, boron reduces the porosity percentage due to the proper growth of SiC grains [22]. One of the compounds in boron and carbon is Boron carbide (B<sub>4</sub>C). Due to its unique properties, B<sub>4</sub>C has a wide range of applications in mechanical, chemical, and

\* Corresponding author. Tel.: +98-9125907184; Fax: +98-21-22970033.  
E-mail address: [alireza.moradkhani@sru.ac.ir](mailto:alireza.moradkhani@sru.ac.ir)

electrical industries such as abrasive manufacturing in polishing equipment, construction of chemical chambers for working with acids and alkalis, and application in various types of thermocouples, and as an additive to other types of nanocomposites [23-28]. The limitation of the use of B<sub>4</sub>C is its high chemical stability, which is mostly due to the difficulty of its sintering because of the strong covalent bond within its crystal lattice [27].

Datta *et al.* [22] showed that adding B<sub>4</sub>C to SiC improved the SiC sintering process and increased the sample density. Stobierski *et al.* [20] found that adding too much B<sub>4</sub>C caused the growth of stretched silicon 4H carbide grains, which reduced the sample density.

When thermal energy is applied to compressed powder, bonds between the particles are established through the process of diffusion mass transport. The driving force of the sinter is the reduction of surface energy by removing the solid-gas joint to increase the solid-solid interface. This free energy causes a significant density because it is associated with the disappearance of small porous [28, 29].

The first investigators who reported SiC powder sintering were Alliegro and his colleagues. They used a hot press to show that additives are required for SiC sintering and that the addition of metals such as iron, aluminum, chromium, calcium, lithium, nickel, boron, aluminum-iron, and zirconium-boron was effective in sintering. Then, in 1975, Prochazka [30] discovered a pressureless sintering method in which small amounts of B and C were added.

In order to perform the pressureless SiC sintering, atomic diffusion must be sufficiently high, and the boundary energy of the recrystallized grains must be low enough to reduce the free energy of the system [28]. Tanaka [28] found that the SiC sintering was successful only in the case that the ratio of surface energy ( $\gamma_{sv}$ ) to the interface energy ( $\gamma_{ss}$ ) was less than 0.7. Uemura *et al.* [31] found that in pure SiC, the ratio of  $\frac{\gamma_{sv}}{\gamma_{ss}}$  was 0.99 due to the covalent bond. The addition of B<sub>4</sub>C with preferential deposition at the SiC grain boundary results in a reduction in

the energy limit of the grain boundary relative to the grain surface energy [32], which ends in providing the energy required for sintering in the solid phase [28]. The possible practical areas for the application of the fabricated materials are car ceramic brakes, fraction discs, medical implants, optical mirrors, heaters and gas turbines, etc. [1-6].

In this study, the mechanical properties, microstructure behavior of formed microstructures, and the fracture behavior of SiC-NanoB<sub>4</sub>C composites with different weight percentages including 0, 0.25, 0.5, 0.75, 1, 2, and 3 wt% nanoB<sub>4</sub>C produced by pressureless sintering were investigated. All samples contained 1wt.% phenolic resin as a source of carbon and binder. In order to compare the results better, sintering duration and temperature, the amount of phenolic resin, the amount of initial press force, and the micron-scale of the B<sub>4</sub>C additive were also considered as variables. The aim of this investigation is allocated to find the best mechanical properties and microstructure of SiC composites by optimizing crucial parameters mentioned in the previous section. In addition, all achieved data is at the highest level such as Relative density in comparison with other articles [28-32], meaning that by optimizing parameters affecting final quality concerned with mechanical and physical properties samples with outstanding applications and properties were achieved.

## 2. Materials and Methods

SiC powder was manufactured by Shandong Qingzhou Micropowder Co. in China and has a purity of 99% with granulated spherical particles with an average size of  $d_{50} = 0.8 \mu\text{m}$ . Table 1 shows the ingredients and impurities of the original SiC and nanoB<sub>4</sub>C powder.

NanoB<sub>4</sub>C powder is made by Chengdu Rong Feng Co. in China with a particle size of 80nm. Figure 1 shows a scanning electron microscopy (SEM) image of nanoB<sub>4</sub>C grains. The MicroB<sub>4</sub>C powder used is also made by the same company with an average particle size of  $d_{50} = 1 \mu\text{m}$ .

**Table 1.** Ingredients of primary powders

Materials	SiC%	%SiO <sub>2</sub>	%C	%B <sub>4</sub> C	%B <sub>2</sub> O <sub>3</sub>	%B	Particle size
SiC	99.9≥	≤0.08	≤0.02	-	-	-	≤0.1 μm
Nano-B <sub>4</sub> C	-	-	-	99.9≥	≤0.09	≤0.01	≤100nm
Micro-B <sub>4</sub> C	-	-	-	99.8≥	≤0.1	≤0.01	≤0.8 μm
α-SiC	99.9≥	≤0.08	≤0.02	-	-	-	≤0.1 μm
β-SiC	99.9≥	≤0.08	≤0.02	-	-	-	≤0.1 μm

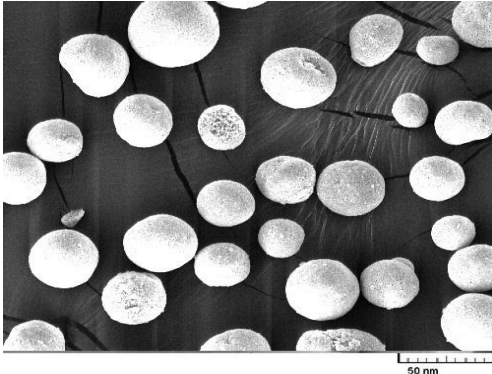


Fig. 1. SEM image of nanoB<sub>4</sub>C primary powder

The phenolic resin powder used has a molecular weight of 134.13  $\frac{gr}{mol}$  and a carbon efficiency of 46%. To measure the materials, a precise powder digital scale made by Sartorius AG, model LA230S, was used. This scale has a weighing accuracy of up to 0.0001 gr and was used to weigh the samples in dry, water-floated, and water-saturated conditions. Table 2 shows the sample code, sintering temperature and duration, press pressure amount, and nano/microB<sub>4</sub>C percentages in the composite.

In order to prepare the samples, the raw materials of each compound were milled in ethanol solution by a planetary ball mill with tanks with tungsten carbide coating and with tungsten carbide pellets with powder to pellets ratio of 1:10 for 3h at 180 rpm. The resulting slurries were then dried at 100°C for 4h. In order to uniform the size of agglomerates, the

compounds are ground in a mortar and passed through a mesh 45 to be prepared for pressing. Sampling was performed by a single-axis hydraulic device. Finally, the samples were prepared in the form of cylindrical pieces with a diameter of 1.2 cm and a height of 0.5 cm. In order to remove glue and volatile materials, all samples were pyrolyzed to a temperature of 600°C at a heating rate of 2°C /min. The sample was then placed in a resistance furnace in an argon atmosphere and heated to a temperature of 2150°C. The heating time was 1.5h and the heating speed was 10°C / min, except for the A8, which was heated to 2200°C for 2h. The samples were cooled naturally in an oven to reach room temperature. The Huser micro-hardness tester was used to apply the Vickers effect on the samples and calculate the hardness level by applying a force of 100-500 gF. The size of the indenter used for measuring the hardness was 1  $\mu$ m. The Vickers indentation method has been used to investigate the length of cracks and assess fracture toughness. Figure 2 illustrates the effect of indenter on SiC composite used for calculating hardness and fracture toughness according to ASTM standards. Tescan electron microscopy with an operating voltage of 15-20 KV was used to study the microstructure and crack growth path in the samples. XRD manufactured by Philips company was used for phase analysis of raw and sintered materials. XRD pattern of the components was obtained in the range of 80-10° with the Cu-K $\alpha$  beam, the nickel filter, and the 40 KV accelerator voltage.

Table 2. Sample codes according to the nano/microB<sub>4</sub>C add-on value and different conditions

Sample	nano B <sub>4</sub> C (%wt)	State of addition B <sub>4</sub> C	Resin phenolic (%wt)	Dwell time (h)	Static Press pressure (MPa)	Temperature (°C) at Argon atmosphere
A1	0	-	1	2	50	2150
A2	0.25	nano	1	2	50	2150
A3	0.5	nano	1	2	50	2150
A4	0.75	nano	1	2	50	2150
A5	1	nano	1	2	50	2150
A6	2	nano	1	2	50	2150
A7	3	nano	1	2	50	2150
A8	0.5	nano	1	3	50	2200
A9	0.5	nano	2	2	50	2150
A10	0.5	micron	1	2	50	2150
A11	0.5	nano	1	2	80	2150

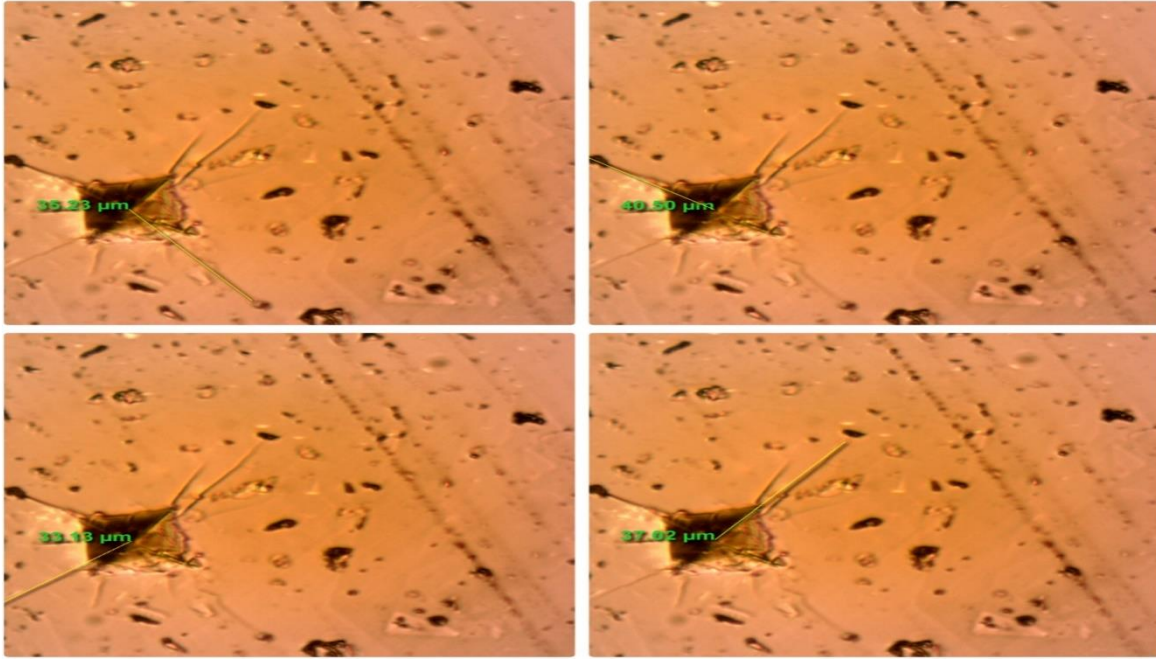


Fig. 2. OM image of SiC composites tested according to ASTM for Hardness and Fracture toughness

The density and porosity of the sintered samples were measured using the Archimedes method and based on the ASTM C373-88 standard [33].

Also, the density of the composite sample theory was measured from equations (1) and (2) according to the Pycnometers method [2], and according to SiC ( $\rho_{SiC}$ ) density equal to 3.21 gr/cm<sup>3</sup> [1-4], B<sub>4</sub>C ( $\rho_{B4C}$ ) density equal to 2.52 gr/cm<sup>3</sup> [24,27] and phenolic resin ( $\rho_R$ ) density equal to 1.32 gr/cm<sup>3</sup> [34].

Where % $V_{SiC}$  is SiC volume fraction, % $V_{B4C}$  is B<sub>4</sub>C volume fraction, and % $V_C$  is Carbon volume fraction. The hardness of the samples was calculated using the Vickers method based on the standard of ASTM C1327 [35]. For this purpose, the surface of the samples was prepared with a polishing machine and polished with diamond up to 1 $\mu$ m. Each sample was subjected to Kg F1 charge for 10s. Five works by Vickers were applied to each sample, and the average was reported as hardness. The modulus of elasticity of the samples was determined based on the ASTM C769 standard [36] and based on changes in the speed of sound in matter with an average of five times measurement. The device used to measure the speed of sound was the TC600 thickness gauge made in Korea (TESTECH). By measuring the velocity with a frequency of 5MHz and the relationship between (1) and (2), Young's modulus was calculated for each sample.

$$E = Y_v \rho v^2 \quad (1)$$

$$Y_v = \frac{(1+v)(1-2v)}{1-v} \quad (2)$$

E is the modulus of elasticity in Pa,  $\rho$  is the density of the sample in gr/cm<sup>3</sup>, v is the speed of sound in the sample in m/s,  $Y_v$  is the factor of

Poisson and  $\nu$  is the Poisson coefficient. The Poisson coefficient of the samples can also be calculated using the law of mixtures and according to Equation (3).

$$\nu = (\nu_{SiC} \times \%V_{SiC}) + (\nu_{B4C} \times \%V_{B4C}) + (\nu_C \times \%V_C) \quad (3)$$

Fracture toughness was obtained based on equation (4) determined by Anstis *et al.* [37].

$$K_{IC} = a \left( \frac{E}{H} \right)^{0.5} \times \left( \frac{P}{c^{3/2}} \right) \quad (4)$$

a is a fixed number independent of matter which was obtained by Anstis that equals 0.016 $\pm$  0.004. E is the modulus of elasticity based on GPa, H is the hardness of the Vickers based on GPa, P is the force exerted to set the effect of the Vickers based on N, and c is the average radial crack length in these evaluations. The mean of the five measurements for each relationship was reported as the fractured index of the samples.

### 3. Results and Discussion

#### 3.1. Microstructure

Figure 3 shows A3 and A8 sample SEM images, respectively. As can be seen, the increasing temperature of the sinter is associated with grain stretching and extreme growth. Increasing the soaking time at 2150 °C also causes the grains to overgrow, increase in porosity, and eventually the reduction of density, meaning that by increasing thermal energy, extra forces are prepared to make grains grow in unwanted directions leading to a reduction in density. Stobierski *et al.* [21] also obtained these results by increasing the percentage of B<sub>4</sub>C in the samples.

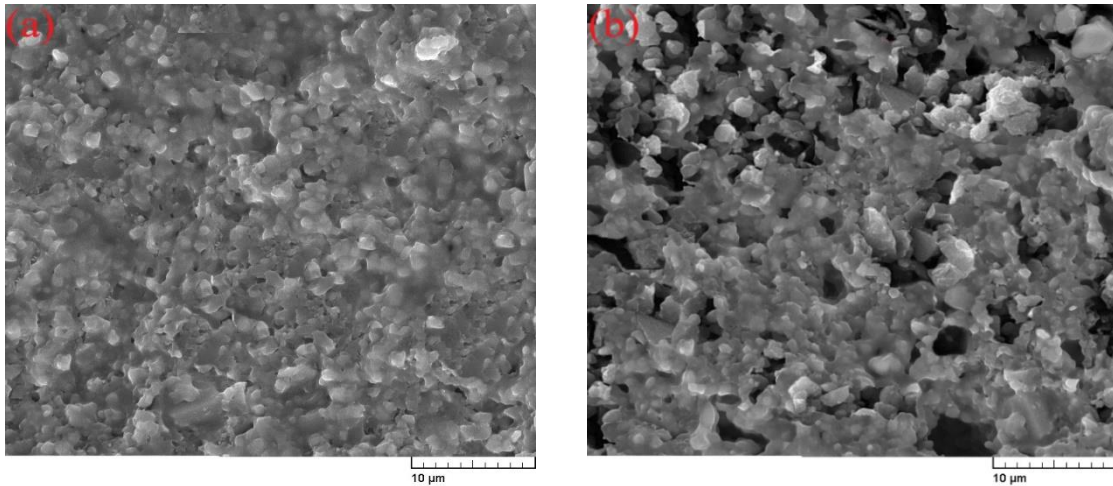


**Fig. 3.** SEM image for samples containing 0.5wt% -nanoB<sub>4</sub>C a) sintered at 2150°C for 2h and b) sintered at 2200°C for 3h

Figure 4-a shows the SEM image of the change in structure from 6H to 4H. As can be seen in Fig. 4-a, increasing the temperature and soaking time increases the grain size in the sample and increases the open and closed porosity of the sample. Increasing the temperature and soaking time creates the energy needed to convert the 6H reaction to 4H [22]. The

The grain structure at 6H is equiaxial and more spherical than 4H. In the 4H structure, the grains are rough and more stretched; Therefore, it causes small cracks and pores around the grains and ultimately reduces the relative density [19]. Figure 4-b shows the XRD pattern of A8 sample. According to it, the results has been approved. Furthermore, Figure 4-c shows the XRD pattern of A3 sample.

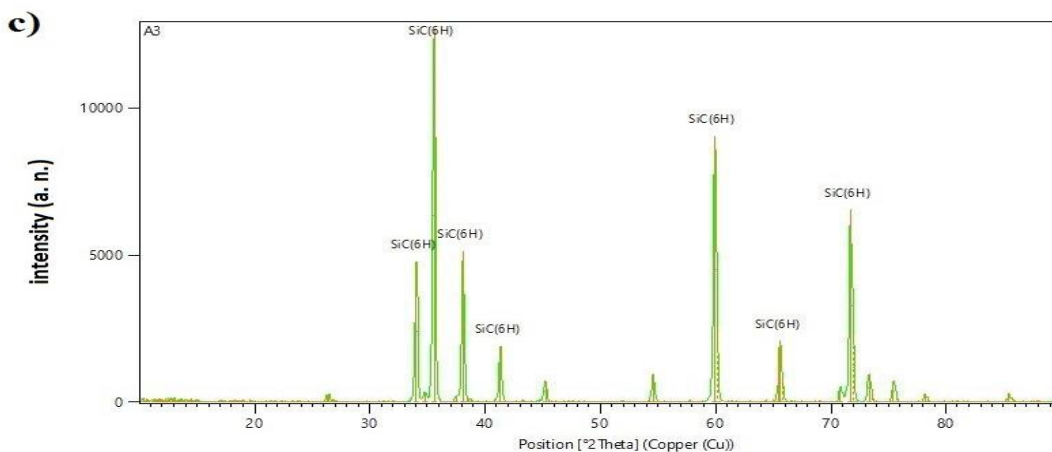
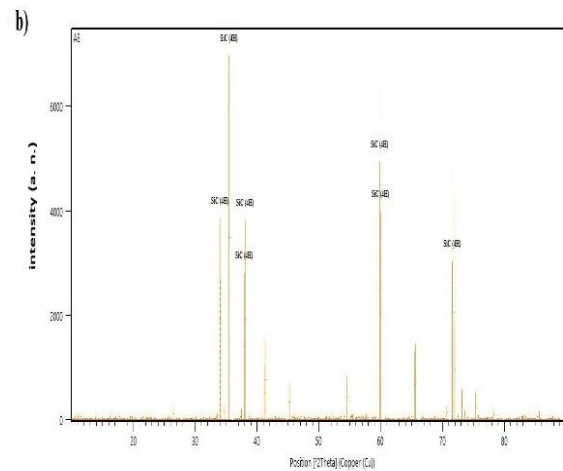
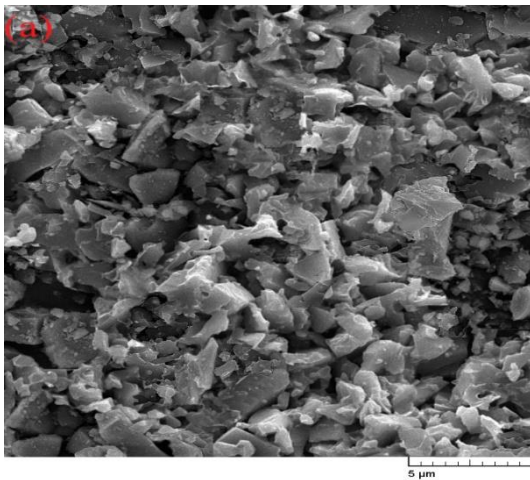
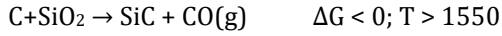


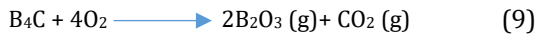
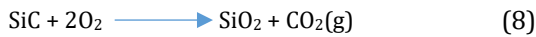
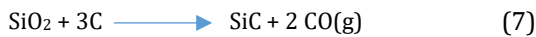
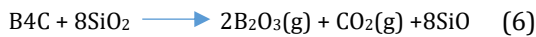
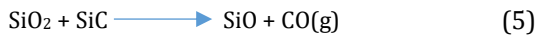
**Fig. 4.** a) SEM image related to the sintered A8 sample at 2200°C and for 3h, the structure of which has changed from 6H to 4H. b) XRD pattern of A8 sample. c) XRD pattern of A3 sample

In the first step of the sintering, a uniform layer including B and O is formed on the SiC. At higher temperatures, C and SiO<sub>2</sub> react and SiC is formed. B disappears from the layers as well as the grain boundaries. As the temperature rises to 2150°C, the thickness of the C layer on the SiC surface decreases, and if the following revival reaction does not take place, carbon remains on the surface of SiC [38].



B penetrates the SiC network. B solution in SiC at 2200°C is about 0.3wt% [38]. As the temperature rises, B from nanoB<sub>4</sub>C begins to combine with C and Si to become SiB<sub>4</sub> and B<sub>4</sub>C, which triggers the release of C and free Si at the grain level. C and Si react together at high temperatures, and sintering occurs. So, in samples that have no nanoB<sub>4</sub>C or less than 0.25% wt, no sintering occurs.

The following important and determining reactions are considered in the SiC sinter for thermal analysis [3, 39].



CO (g) and O<sub>2</sub> (g) are harmful to the system [39]. Because in addition to increasing the entropy of the system and producing many moles of the gas phase [3], they oxidize SiC and B<sub>4</sub>C and destroy furnace elements at high temperatures [39]. B<sub>2</sub>O<sub>3</sub> as a gas reduces the activity of SiC granules and density by sitting on the surface [3].

When B<sub>2</sub>O<sub>3</sub> (g) exits, On the other hand, it causes closed and open porosity throughout the sample and the percentage of porosity increases [39]. Reactions that are beneficial to the system should be performed at a low rate of heating.

According to equation (10), nanoB<sub>4</sub>C reduces the amount of activation energy for grain growth, therefore, makes the grain smaller and increases the strength of the composite. In equation (10), D is the grain size after heat treatment, D<sub>0</sub> is the grain size of the primary grain and Q<sub>G</sub> is the activation energy for growth [21].

$$D^n - D_0^n = k t \exp (-Q_G/RT) \quad (10)$$

The use of nanoB<sub>4</sub>C creates stronger chemical bonds between the basic material and the secondary phase, due to the increase in the surface area followed by the increase in activity, which eventually increases the strength of the composite [38]. In addition to increasing the particle level, it reduces the surface pressure and results in a change in the distance between the particles or the distance between the atoms of the particles. On the other hand, according to equation 11, which is known as the hall-petch relationship, it can be argued that as the grain size decreases, the initial phase is amplified and becomes stronger [39].

$$\sigma_Y = \sigma_0 + \frac{k}{\sqrt{d}} \quad (11)$$

$\sigma_Y$  is the material yield strength,  $\sigma_0$  is the frictional stress of the network,  $K$  is the constant and coefficient value that depends on the accumulation of misalignments in the grain boundary and  $d$  is the size of the crystal grains.

In fig 5-c it has been shown that As the dwelling time increases, the grain size rises, and the grains are likely to grow intensively, change the 6H to 4H allotropy, and the grain structure changes from the equiaxial shape to the elongated shape [22].

### 3.2. Relative Density and Porosity

Table 3 shows the raw density and relative density of the samples. As you can see, as the percentage of carbon and the plasticity of the powder increases, the raw density goes up. However, with increasing nanoB<sub>4</sub>C percentage, ceramic as a hard phase causes residual stress as well as open and closed porosity due to the application of pressure and reduction of the raw density of the samples. The 2.6% reduction in the A1 and A7 models is due to the pressure applied around the nanoB<sub>4</sub>C particle. Increased B<sub>4</sub>C in the form of nanoparticles can cause agglomeration if not fully mixed and properly milled. It also prevents proper pressing and creates very large pores in the sample, which leads to a decrease in mechanical properties and relative density [39]. Boron increases C and Si diffusion rates, which results in a better SiC density [38]. In SiC, the  $\epsilon_b/\epsilon_s$  ratio (surface energy to grain boundary energy ratio) should be less than 0.7. Density needs to reduce  $\epsilon_b$  with the help of sintering. The role of the sinter as help is to reduce the energy in the grain border. Adding B reduces the energy in the grain boundary, i.e., it reduces  $\epsilon_b$ , and grain boundary energy by depositing in the grain boundary [38, 21].

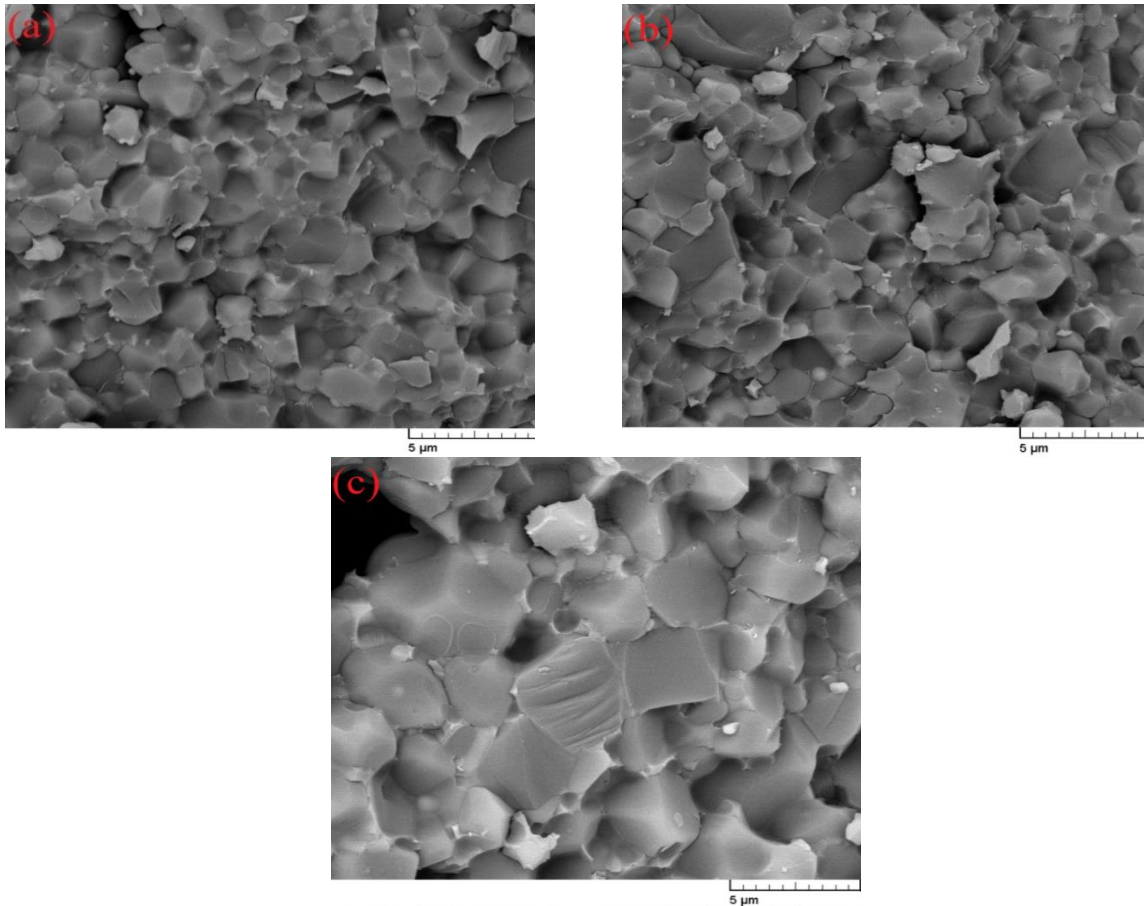


Fig. 5. a) SEM image related to A3 b) SEM image related to A10 c) SEM image related to the A8 sintered at 2200°C and for 3h, the structure of which has changed from 6H to 4H

In sintering operations, the soaking time at maximum temperature is one of the most important parameters affecting the relative density [1-5, 28]. As the soaking time increases, the grain size increases and the grains are likely to grow intensively, causing porosity and reduced relative density. In addition, as the soaking time increases, the energy required to change the 6H to 4H allotropy is provided, the grain structure changes from the equiaxed shape to the elongated shape with porosity, and the relative density decreases [22].

**Table 3.** Raw and relative density values of SiC-nano / microB4C composite samples

samples	Raw density (%)	Relative density (%)	theoretical density (gr/cm <sup>3</sup> )
A1	60.7	80.98	3.20
A2	59.9	95.36	3.20
A3	59.8	98.32	3.19
A4	59.6	96.06	3.19
A5	59.3	93.81	3.18
A6	58.5	91.11	3.17
A7	58.1	89.12	3.16
A8	59.8	95.47	3.19
A9	60.3	94.89	3.19
A10	59.7	98.23	3.19
A11	61.1	94.03	3.19

Due to the lack of nanoB<sub>4</sub>C additives, in sample A1, sintering has not or has rarely been performed. The density is 80.98 %, which is very low compared to the optimal value of 98.32 %. In the A2 sample, as the percentage of additive increases, nanoB<sub>4</sub>C acts as a germinator and increases the density and operation of sintering. In the A3 model, which has the highest relative density of 98.32% and the lowest porosity, the full sintering operation is performed.

From sample A4 to sample A7, an increase in the percentage of secondary nanoB<sub>4</sub>C phase in the composite microstructure of elongated grains and more porosity is observed. This also reduces the relative density and increases the porosity at the sample level. In addition to these factors, with increasing nanoB<sub>4</sub>C percentage, B<sub>2</sub>O<sub>3</sub> production increases [28], which leads to gas leakage from the samples and porosity. Although the A8 model has 0.5 wt.% nanoB<sub>4</sub>C, it causes the gains to grow excessively, converts 6H to 4H, makes the grains more stretched, and creates porosity, it causes the grains to grow excessively, converting 6H to 4H, making the grains more elongated, and creating porosity due to the increase in the time and temperature of the sinter.

In the A9 sample, as the percentage of phenolic resin increased to 2% by weight, carbon

deposited in the grain boundaries, prevented mass transfer, sintering was not fully done, and the density dropped sharply [29]. Comparing the values obtained in sample A10 where B<sub>4</sub>C is added as a micron, it is observed that the addition of NanoB<sub>4</sub>C increases the surface ratio and reactivity. As a result, stronger chemical bonds are formed between SiC and other particles. In addition, as the B<sub>4</sub>C particles become smaller, the nucleation site grows and the base becomes finer. In the A11 sample, taken into account that the press pressure is higher than the other samples, the raw density increases significantly by 1.3% compared to the A3 sample. However, after the sintering operation, due to the creation of small pores throughout the sample, a relatively proper density has not been obtained. Also, compared to the results of Li *et al* [40], in which SiC sintering was performed using the SPS method, the obtained results are better, which could be due to the use of nanoB<sub>4</sub>C.

Pyrolysis causes the volatile substances in the primary powder to slowly evaporate and also prevents porosity during the sintering operation [41]. In addition, the stress caused by static and even isostatic pressure is largely removed from the sample [1-4, 39]. Without the pyrolysis process, residual stresses around the nanoB<sub>4</sub>C particles cause cracks and porosity, which reduce the relative density [1-4].

### 3.3. Hardness

Figure 6 shows the hardness values of the samples. As can be seen, increasing the nanoB<sub>4</sub>C percentage from 0 to 0.5% wt increases the hardness rate to 28.6 GPa, and increasing the nanoB<sub>4</sub>C percentage by increasing the porosity, reduces the hardness by 18%. By comparing the hardness and relative density, it can be seen that by reducing the relative density and increasing the porosity, the hardness decreases. Also, increasing the duration of sintering with a similar mechanism reduces the hardness of the samples [21]. The higher the hardness of the constituent phase, the more the hardness increases, provided that it does not cause porosity in the grains and around the grain boundaries [21, 1-2]. On the other hand, during cooling after sintering in the furnace and due to the difference in volumetric expansion coefficients of nanoB<sub>4</sub>C and SiC, residual stresses and micro-cracks are created around the reinforcements, which reduces the hardness [42]. In addition, based on equation (10), decreasing particle size leads to its strength, and hardness [39].

Since the A1 model is without nanoB<sub>4</sub>C, it has a lot of porosity, which indicates improper sintering. In the A2 sample, with an increase in the percentage of nanoB<sub>4</sub>C, we see an increase in hardness of 0.25 GPa in the sample, which is

probably due to the presence of nanoB<sub>4</sub>C in the sample, which helps reduce porosity through increasing sintering. A4 has the lowest percentage of porosity and the highest relative density. Also, it has the highest amount of hardness due to the finer grain size of the composite, the increase in the amount of grain boundary phase in the sample, the increase in the percentage of nanoB<sub>4</sub>C secondary phase compared to the previous samples, and also the elimination of porosity. From the A4 to the A7, which is featured by an increase in the percentage of hard phase, the grains change from equiaxial shape to become stretched. This reduces the grain boundary phase and also creates pores around the grain and grain boundary [19, 22]. In these samples, the mechanism of increasing the hardness is the result of increasing the hard phase due to a rise in the percentage of nanoB<sub>4</sub>C that enhances the porosity and stretching of the grains and practically causes a decrease in mechanical properties. In addition, by increasing the percentage of nanoB<sub>4</sub>C, the hardness rate is reduced as the result of the residual stress added to the raw samples due to the pressure of the hydraulic press and the reduction of powder plasticity and pressability. In the A8 sample, as the temperature of the sinter and the soaking time increases, hardness decreases probably due to the overgrowth of the grains and the formation of porosity and reduction of the grain boundary phase. In the A9 sample, as the percentage of phenolic resin increased, carbon precipitated in the grain boundaries, preventing mass transfer and causing porosity throughout the sample and a severe drop in hardness. In the A10 model, by adding a B<sub>4</sub>C on a micron scale, the level of additive contact is lower than in the Nano mode, which leads to a reduction in hardness. Comparing the results of the hardness level in the A3 sample and Li *et al* [40] research on the SiC-B<sub>4</sub>C composite sintering, we find an achieved hardness of 28.5 GPa; The A3 sample had 0.3% better results.

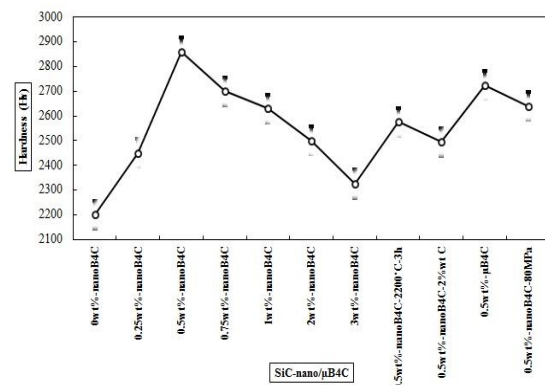


Fig. 6. Vickers hardness of SiC-B<sub>4</sub>C samples based on increasing B<sub>4</sub>C weight percentage and other parameters

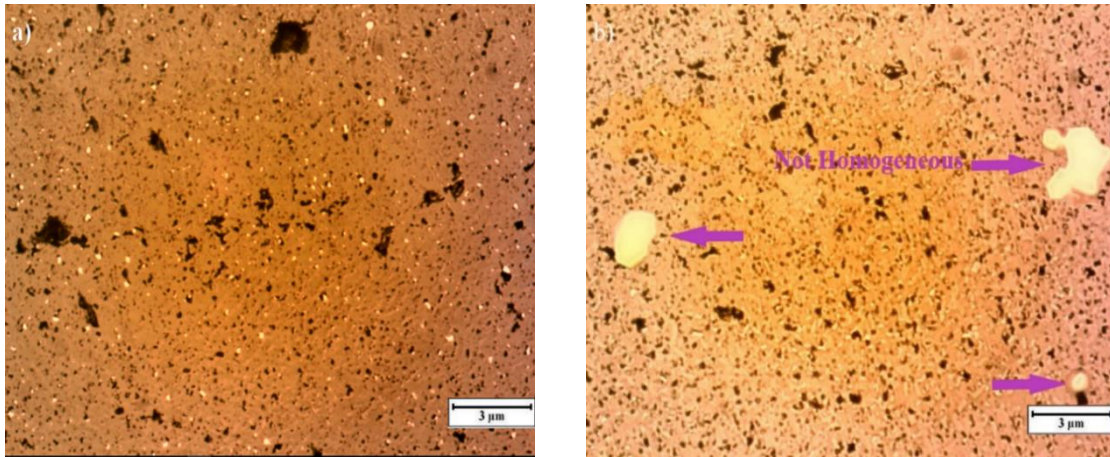


Fig. 7. OM image containing 0.5%wt B<sub>4</sub>C a) nanoB<sub>4</sub>C b) microB<sub>4</sub>C

Figure 7 shows the difference in homogeneity due to the use of mill in micron and nano samples containing 0.5% wt B<sub>4</sub>C. As can be seen, the smaller the grain size, the hard phase of the grain boundary increases [39]. Moreover, due to the presence of nanoB<sub>4</sub>C in the grain boundaries, grain size decreases, and hardness increases [38]. Also, the smaller the particles, the amount of nanoB<sub>4</sub>C as germinant increases which leads to finer primary phase grains and an increase in grain boundaries and hardness. [40].

### 3.4. Young's Modulus

In Fig. 8, the values of the young's modulus of the samples can be seen. Sample A1 has the lowest amount of Young's modulus because the sintering process has not been completed and the %wt-B<sub>4</sub>C is zero in this sample. Also, due to the same reason and lack of %wt-B<sub>4</sub>C in the A2 sample, there is a big difference of about 10% with the optimal A3 sample. It is obvious that the A3 model has the best percentage of porosity and relative density, the spherical state of the grain, with the best sound speed, and Young's modulus. Increasing the percentage of nanoB<sub>4</sub>C in the A4 to A7 samples reduces the speed of sound and young's modulus due to the relative decrease in density and porosity, as well as the excessive deposition of nanoB<sub>4</sub>C in the grain boundary and thickening of the grain boundary. As the percentage of porosity in the specimens increases, the speed of sound, and thus the modulus of young decreases. [39] In general, any factor that reduces the number of grain boundaries or makes them thinner and increases the speed of sound [39]. The speed of sound in nanoB<sub>4</sub>C is higher than the speed of sound in SiC [1]. Therefore, with increasing nanoB<sub>4</sub>C percentage, the speed of sound increases. On the other hand, with a further increase of nanoB<sub>4</sub>C, the porosity also increases, which has a greater effect on the speed of sound [21]. In the A9 model, the porosity increases, and the speed of sound

decreases due to carbon deposition in the grain boundary and no mass transfer, and as a result, the amount of Young's modulus decreases.

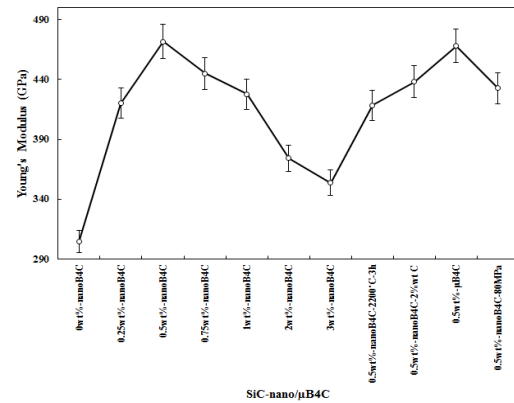


Fig. 8. Young's modulus of SiC-B<sub>4</sub>C samples by increasing B<sub>4</sub>C weight percentage and other parameters

Moreover, according to equation (12), any factor that increases the porosity percentage causes a reduction in Young's modulus.

$$E = E_0 (1 - 1.9P + 0.9P^2) \quad (12)$$

E is equal to the final Young's modulus, E<sub>0</sub> shows the value of the theory Young's modulus for the ideal sample, and P represents the percentage of porosity in the sample [39].

By increasing the percentage of carbon and due to the deposition of carbon in the grain boundary and preventing the transfer of mass, the porosity in the sample increases, and Young's modulus decreases. According to the law of mixtures and based on the relation (13), E<sub>B4C</sub> is more than E<sub>SiC</sub> and E<sub>C</sub>, and with increasing carbon content, Young's modulus also increases. Because the presence of the nanoB<sub>4</sub>C phase in the grain boundaries makes them thinner, which leads to an increase in the speed of sound in the grain boundaries. Therefore, nanoB<sub>4</sub>C improves the sound speed and young's modulus compared to microB<sub>4</sub>C. On the other hand, increasing the percentage of nanoB<sub>4</sub>C (more than 0.5% wt) also

increases the porosity and reduces the speed of sound.

$$E = (E_{SiC} \times \%V_{SiC}) + (E_{B4C} \times \%V_{B4C}) + (E_C \times \%V_C) \quad (13)$$

### 3.5. Fracture Toughness

Figure 9 shows the fracture toughness values in samples calculated for relation (4). From samples A1 to A3, fracture toughness has increased because of an increase in nanoB<sub>4</sub>C due to enhanced relative density and reduced porosity in the samples. Also, there is a decrease in fracture toughness from samples A4 to A7 due to increased porosity. A more homogeneous presence of nanoB<sub>4</sub>C, due to the prevention of cracking and dealing with it, reduces the crack length and increases the fracture toughness. Mechanisms for this increase include bypassing crack, stopping crack, branching crack, bridging crack, and deflection crack [43-54].

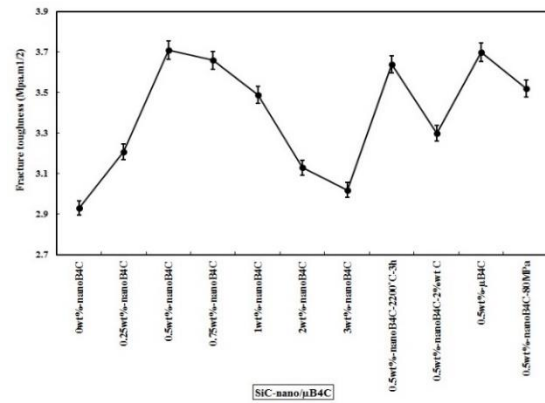


Fig. 9. The fracture toughness index of SiC-B<sub>4</sub>C samples by weight gain of B<sub>4</sub>C and other parameters obtained from equation 4.

Figure 10 shows the various mechanisms for increasing the fracture toughness index in sample A3 with 0.5% wt-nanoB<sub>4</sub>C, which has improved fracture toughness values in this sample. As shown, the red arrows are deflection cracks and the blue indicates bridging cracks.

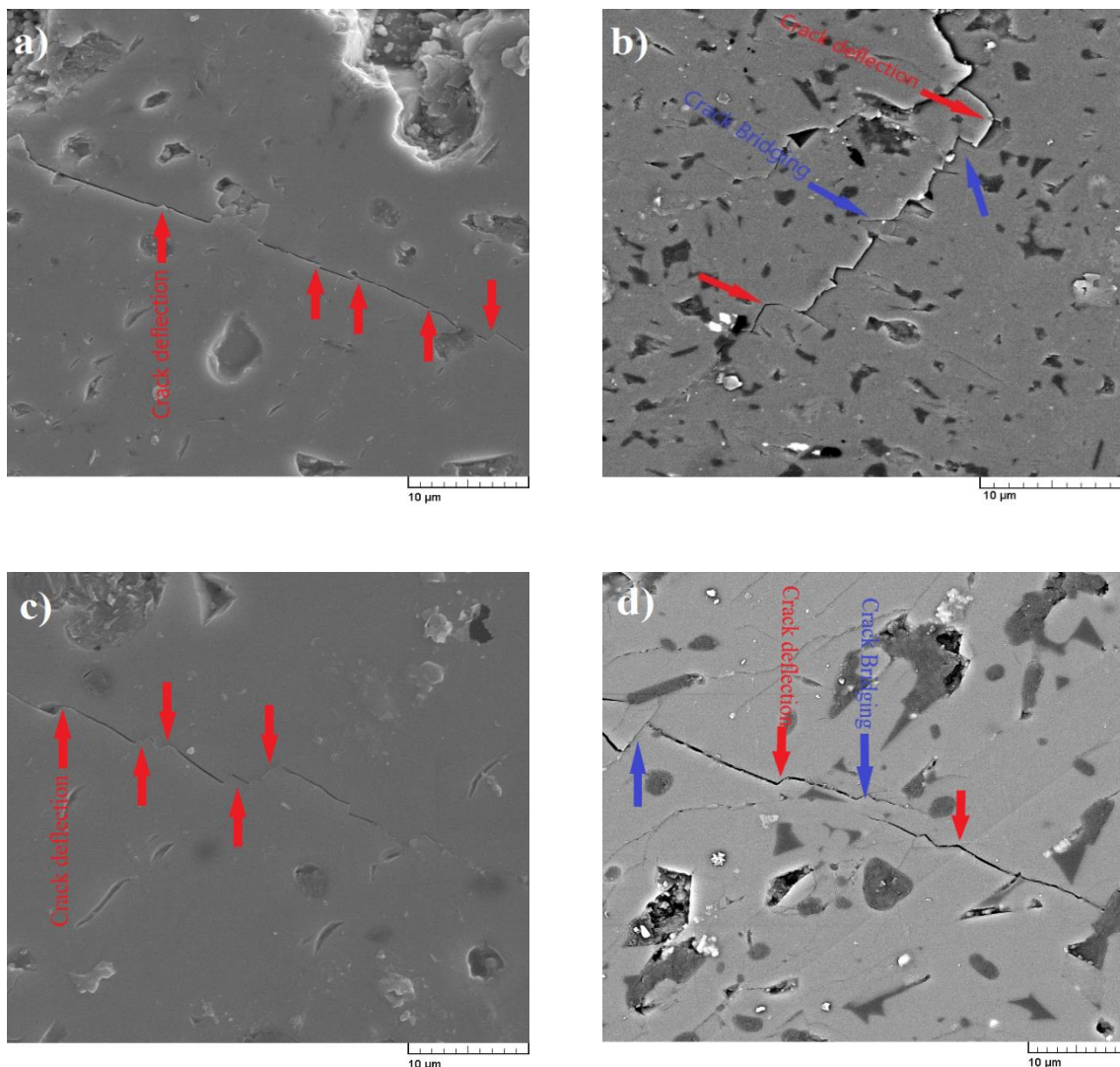
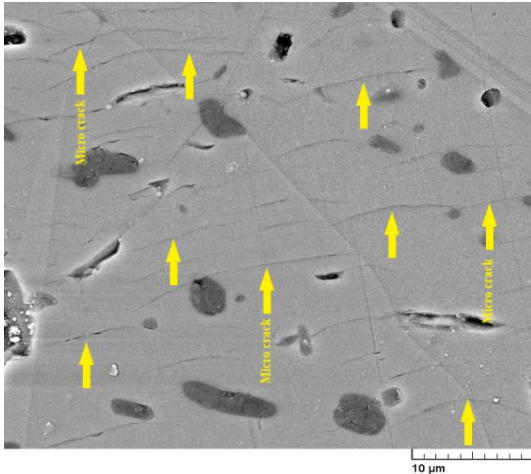


Fig. 10. SEM image of sample A3 additive 0.5 wt%-nanoB<sub>4</sub>C a) deflection cracks b) Bridging and deflection cracks c) deflection cracks d) Bridging and deflection cracks (Red arrows are deflection cracks and blue indicates bridging cracks)

Figure 11 of the SEM image shows a sample with an operating pressure of 80 MPa in sample A11. As can be seen, at the sample level, some micro-cracks are probably caused by increased pressure in the press. As the pressure increases, there appears a difference in the SiC and nanoB<sub>4</sub>C volume expansion coefficients, and the residual stress and micro-cracks are formed around the secondary phase. They vary in size depending on the length of the microcracks and have different effects as shown in Fig. 11.



**Fig. 11.** SEM image of sample A11 with 80 MPa static pressure. Microcracks are created by increasing the amount of static pressure

### 3.6. Fracture Mode

Because grain boundaries are often the gathering place for faults and irregularities, the probability of inter-grain fracture is higher [1-4, 46]. Figures 12 and 13 show the types of fractures in sample composites A1 and A3, respectively. As can be seen in Fig. 12, due to the incompleteness of the sintering process, the bond between the particles is weaker than other samples, and this is the reason for the intergranular fracture in this sample [55, 56].

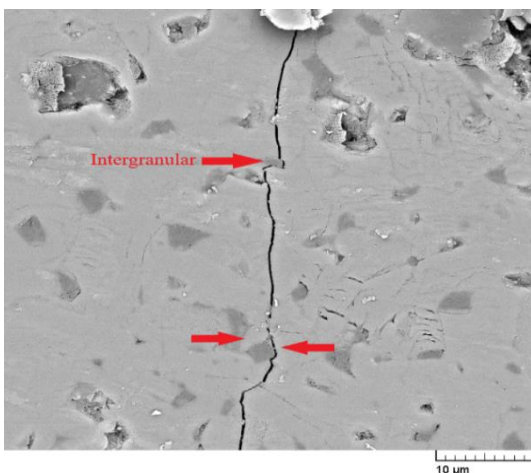


**Fig. 12.** SEM image of sample A1 without the addition of nanoB<sub>4</sub>C, the fracture of which is intergranular.

As nanoB<sub>4</sub>C increases and the intergranular bond in this composite becomes stronger, the fracture mode changes from intergranular to transgranular, as shown in Fig. 13. This indicates that the bond between the particles formed in the sintering stage is stronger [57- 60].

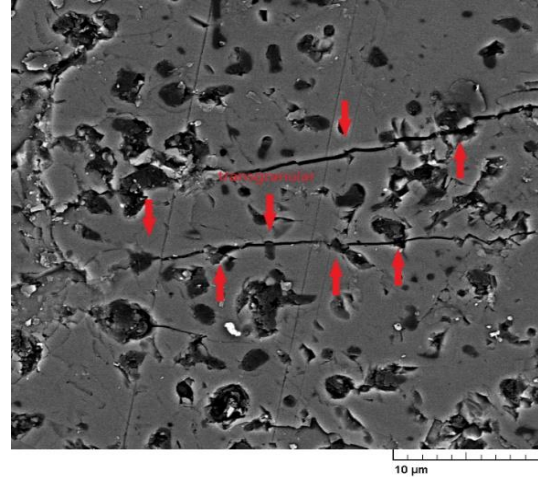


**Fig. 13.** SEM image of sample A3 with the addition of 0.5% wt-nanoB<sub>4</sub>C, which is a transgranular fracture.

## 4. Conclusions

In this study, the mechanical properties and microstructure of SiC-NanoB<sub>4</sub>C composites with different weight percentages of NanoB<sub>4</sub>C made by the pressureless sintering method have been investigated. The following results have been obtained:

- With the increase in nanoB<sub>4</sub>C additives from 0% wt to 0.5% wt, the relative density has increased from 81.32% to 98.77%. A further increase in nanoB<sub>4</sub>C additives to 3% wt leads to a relative density of 89.47%.
- With the addition of nanoB<sub>4</sub>C additives from 0% wt to 0.5% wt, the hardness rate has risen from 22 GPa to 28.6 GPa. A further increase in nanoB<sub>4</sub>C additives to 3% wt reduces the hardness by 18%.
- The Young's modulus amount in the SiC-0.5% wt-nanoB<sub>4</sub>C model has reached 471.822 GPa, an increase of 54% over the non-additive sample. A further increase in nanoB<sub>4</sub>C additives to 3% wt reduced young's module by 25%.
- With the addition of nanoB<sub>4</sub>C additives from 0% wt to 0.5% wt, the fracture toughness value increases from 2.93 MPa.√m to 3.71 MPa.√m (26%). A further rise in the nanoB<sub>4</sub>C additive to 3%wt reduces the fracture toughness index by 18%.
- Nano-sized B<sub>4</sub>C additive particles have a higher surface-to-volume ratio than micronized particles; This causes a higher

level of reaction with the base, which leads to increased sinterability and mechanical properties of the composite.

- With increasing nanoB<sub>4</sub>C additives from 0% wt to 0.5% wt, the fracture in the sample has changed from intergranular to transgranular, which indicates an improvement in mechanical properties.
- By increasing the percentage of nanoB<sub>4</sub>C and converting 6H to 4H, making the grains more stretched, and creating porosity due to the increase in the time and temperature of the sinter.

### Conflicts of Interest

The authors declare that there is no conflict of interest regarding the publication of this paper.

### References

- [1] Liu, Q., Li, Y. and Xiao, W., 2019. Oxygen impurity effects on the mechanical properties of SiC studied by first principles calculations. *Materials Today Communications*, 19, pp.360-365.
- [2] Harris, G.L., 1995. Properties of silicon carbide, INSPEC. *The Institution of Electrical Engineers, London*, 5.
- [3] Kimoto, T. and Cooper, J.A., 2014. *Fundamentals of silicon carbide technology: growth, characterization, devices and applications*. John Wiley & Sons.
- [4] Somiya, S., Inomata Y., 1991. Silicon carbide ceramics. 1. Fundamental and solid reaction, Springer.
- [5] Williams, T., 2016. *Development of pressureless sintered silicon carbide-boron carbide composites for armour applications*. University of Surrey (United Kingdom).
- [6] Rivera, K. and Gregory, O.J., 2020. ITO: SiC Ceramic Matrix Composite Thermocouples for Engine Components. *IEEE Sensors Letters*, 4(5), pp.1-4.
- [7] Graziani, T., Baxter, D.J. and Nannetti, C.A., 1996. Degradation of silicon carbide-based materials in a high temperature combustion environment. In *Key Engineering Materials* (Vol. 113, pp. 153-166). Trans Tech Publications Ltd.
- [8] Hotza, D., Di Luccio, M., Wilhelm, M., Iwamoto, Y., Bernard, S. and da Costa, J.C.D., 2020. Silicon carbide filters and porous membranes: A review of processing, properties, performance and application. *Journal of Membrane Science*, 610, p.118193.
- [9] Natarajan, H.K., 2018. Study of silicon carbide-reinforced aluminum matrix composite brake rotor for motorcycle application. *The International Journal of Advanced Manufacturing Technology*, 94(1), pp.1461-1475.
- [10] Gryshkov, O., Klyui, N.I., Temchenko, V.P., Kyselov, V.S., Chatterjee, A., Belyaev, A.E., Lauterboeck, L., Iarmolenko, D. and Glasmacher, B., 2016. Porous biomorphic silicon carbide ceramics coated with hydroxyapatite as prospective materials for bone implants. *Materials Science and Engineering: C*, 68, pp.143-152.
- [11] Ding, G., He, R., Zhang, K., Zhou, N. and Xu, H., 2020. Stereolithography 3D printing of SiC ceramic with potential for lightweight optical mirror. *Ceramics International*, 46(11), pp.18785-18790.
- [12] Tu, Z., Mao, J., Jiang, H., Han, X. and He, Z., 2017. Numerical method for the thermal analysis of a ceramic matrix composite turbine vane considering the spatial variation of the anisotropic thermal conductivity. *Applied Thermal Engineering*, 127, pp.436-452.
- [13] Lipowitz, J., Rabe, J.A., Zangvil, A. and Xu, Y., 1997, January. Structure and properties of Sylramic™ silicon carbide fiber—A polycrystalline, stoichiometric  $\beta$ -SiC composition. In *Proceedings of the 21st Annual Conference on Composites, Advanced Ceramics, Materials, and Structures—A: Ceramic Engineering and Science Proceedings* (pp. 147-157). Hoboken, NJ, USA: John Wiley & Sons, Inc.
- [14] Shen, G., Bando, Y., Ye, C., Liu, B. and Golberg, D., 2006. Synthesis, characterization and field-emission properties of bamboo-like  $\beta$ -SiC nanowires. *Nanotechnology*, 17(14), p.3468.
- [15] Zhou, X.T., Lai, H.L., Peng, H.Y., Au, F.C., Liao, L.S., Wang, N., Bello, I., Lee, C.S. and Lee, S.T., 2000. Thin  $\beta$ -SiC nanorods and their field emission properties. *Chemical Physics Letters*, 318(1-3), pp.58-62.
- [16] Shigeta, M., Suzuki, A., Furukawa K., Fujii, Y., 1994. Method for the growth of silicon carbide single crystals, Google Patents.
- [17] Li, J., Porter, L. and Yip, S., 1998. Atomistic modeling of finite-temperature properties of crystalline  $\beta$ -SiC: II. Thermal conductivity and effects of point defects. *Journal of Nuclear Materials*, 255(2-3), pp.139-152.
- [18] Gulden, T.D., 1969. Mechanical Properties of Polycrystalline  $\beta$ -SiC. *Journal of the American Ceramic Society*, 52(11), pp.585-590.
- [19] Magnani, G., Beltrami, G., Minoccari, G.L. and Pilotti, L., 2001. Pressureless sintering and properties of  $\alpha$ -SiC-B<sub>4</sub>C composite. *Journal of the European Ceramic Society*, 21(5), pp.633-638.

- [20] Stobierski, L. and Gubernat, A., 2003. Sintering of silicon carbide. Effect of carbon. *Ceramics international*, 29(3), pp.287-292.
- [21] Stobierski, L. and Gubernat, A., 2003. Sintering of silicon carbide II. Effect of boron. *Ceramics international*, 29(4), pp.355-361.
- [22] Datta, M.S., Bandyopadhyay, A.K. and Chaudhuri, B., 2002. Sintering of nano crystalline  $\alpha$  silicon carbide by doping with boron carbide. *Bulletin of Materials Science*, 25(3), pp.181-189.
- [23] Guo, H., Sciora, P., Kooyman, T., Buiron, L. and Rimpault, G., 2019. Application of boron carbide as burnable poison in sodium fast reactors. *Nuclear Technology*, 205(11), pp.1433-1446.
- [24] Cao, X., Shang, L., Liang, Y., Lu, Z., Zhang, G. and Xue, Q., 2020. Tribological performances of the boron carbide coatings sliding against silicon carbide and silicon nitride balls under various relative humidity conditions. *Ceramics International*, 46(3), pp.3074-3081.
- [25] Li, X., Jiang, D., Zhang, J., Lin, Q., Chen, Z. and Huang, Z., 2014. Pressureless sintering of boron carbide with Cr<sub>3</sub>C<sub>2</sub> as sintering additive. *Journal of the European Ceramic Society*, 34(5), pp.1073-1081.
- [26] Cao, X., Wang, J., Liang, Y., Zhang, G., Shang, L., Lu, Z. and Xue, Q., 2020. Corrosion and tribological investigations of the B<sub>4</sub>C coatings rubbing against SiC ball for high relative humidity engineering application. *Materials Today Communications*, 23, p.100924.
- [27] Shi, L., Gu, Y., Chen, L., Qian, Y., Yang, Z. and Ma, J., 2003. A low temperature synthesis of crystalline B<sub>4</sub>C ultrafine powders. *Solid state communications*, 128(1), pp.5-7.
- [28] Tanaka, H., 1991. Sintering of silicon carbide. In *Silicon Carbide Ceramics-1* (pp. 213-238). Springer, Dordrecht.
- [29] Alliegro, R.A., Coffin, L.B. and Tinklepaugh, J.R., 1956. Pressure-sintered silicon carbide. *Journal of the American Ceramic Society*, 39(11), pp.386-389.
- [30] PROCHAZKA, S. and SCANLAN, R.M., 1975. Effect of boron and carbon on sintering of SiC. *Journal of the American Ceramic Society*, 58(1-2), pp.72-72.
- [31] Uemura, Y., Inomata, Y. and Ichinose, H., 1987. Boundary structures of SiC bicrystal. *YOGYO-KYOKAI-SHI*, 95(9), pp.841-844.
- [32] Moradkhani, A. and Baharvandi, H., 2018. Mechanical properties and fracture behavior of B<sub>4</sub>C-nano/micro SiC composites produced by pressureless sintering. *International Journal of Refractory Metals and Hard Materials*, 70, pp.107-115.
- [33] Tam, C.H., Lee, S.C., Chang, S.H. and TAI, F.C., 2008. ASTM C373-88 15.02 ASTM C373-88 15.02, 2006. *Materials transactions*, 49(2), pp.382-386.
- [34] Pappas, J., Patel, K. and Nauman, E.B., 2005. Structure and properties of phenolic resin/nanoclay composites synthesized by in situ polymerization. *Journal of applied polymer science*, 95(5), pp.1169-1174.
- [35] ASTM, C., 2008. 1327-08. Standard test method for Vickers indentation hardness of advanced ceramics. *Annual Book of ASTM Standards*.
- [36] ASTM C769, 2015. Standard Test Method for Sonic Velocity in Manufactured Carbon and Graphite Materials for Use in Obtaining an Approximate Value of Young's Modulus. DOI: 10.1520/C0769-15.
- [37] Anstis, G.R., Chantikul, P., Lawn, B.R. and Marshall, D.B., 1981. A critical evaluation of indentation techniques for measuring fracture toughness: I, direct crack measurements. *Journal of the American Ceramic Society*, 64(9), pp.533-538.
- [38] Wroblewska, G.H., Nold, E. and Thümmel, F., 1990. The role of boron and carbon additions on the microstructural development of pressureless sintered silicon carbide. *Ceramics international*, 16(4), pp.201-209.
- [39] Kingery, W.D., Bowen, H.K. and Uhlmann, D.R., 1976. *Introduction to ceramics* (Vol. 17). John Wiley & Sons.
- [40] Li, C., Li, S., An, D. and Xie, Z., 2020. Microstructure and mechanical properties of spark plasma sintered SiC ceramics aided by B<sub>4</sub>C. *Ceramics International*, 46(8), pp.10142-10146.
- [41] Rödel, J., 1992. Interaction between crack deflection and crack bridging. *Journal of the European Ceramic Society*, 10(3), pp.143-150.
- [42] Snead, L.L., Nozawa, T., Katoh, Y., Byun, T.S., Kondo, S. and Petti, D.A., 2007. Handbook of SiC properties for fuel performance modeling. *Journal of nuclear materials*, 371(1-3), pp.329-377.
- [43] Moradkhani, A., Baharvandi, H. and Naserifar, A., 2019. Effect of sintering temperature on the grain size and mechanical properties of Al<sub>2</sub>O<sub>3</sub>-SiC Nanocomposites. *Journal of the Korean Ceramic Society*, 56(3), pp.256-268.
- [44] Moradkhani, A. and Baharvandi, H., 2017. Determining the fracture resistance of B<sub>4</sub>C-NanoSiB<sub>6</sub> nanocomposite by Vickers indentation method and exploring its mechanical properties. *International Journal*

- of *Refractory Metals and Hard Materials*, 68, pp.159-165.
- [45] Moradkhani, A. and Baharvandi, H., 2018. Effects of additive amount, testing method, fabrication process and sintering temperature on the mechanical properties of Al<sub>2</sub>O<sub>3</sub>/3Y-TZP composites. *Engineering Fracture Mechanics*, 191, pp.446-460.
- [46] Moradkhani, A. and Baharvandi, H., 2018. Analyzing the microstructures of W-ZrC composites fabricated through reaction sintering and determining their fracture toughness values by using the SENB and VIF methods. *Engineering Fracture Mechanics*, 189, pp.501-513.
- [47] Becher, P.F., 1991. Crack bridging processes in toughened ceramics. In *Toughening Mechanisms in Quasi-Brittle Materials* (pp. 19-33). Springer, Dordrecht.
- [48] Kovar, D., Thouless, M.D. and Halloran, J.W., 1998. Crack deflection and propagation in layered silicon nitride/boron nitride ceramics. *Journal of the American Ceramic Society*, 81(4), pp.1004-1112.
- [49] Kabel, J., Hosemann, P., Zayachuk, Y., Armstrong, D.E., Koyanagi, T., Katoh, Y. and Deck, C., 2018. Ceramic composites: A review of toughening mechanisms and demonstration of micropillar compression for interface property extraction. *Journal of materials research*, 33(4), pp.424-439.
- [50] Li, B., 2012. Effect of toughening mechanisms of crack bridging on ceramic materials. In *Advanced Materials Research* (Vol. 476, pp. 1071-1074). Trans Tech Publications Ltd.
- [51] Rice, R.W., 2000. *Mechanical properties of ceramics and composites: grain and particle effects*. CRC Press.
- [52] Ohji, T., Jeong, Y.K., Choa, Y.H. and Niihara, K., 1998. Strengthening and toughening mechanisms of ceramic nanocomposites. *Journal of the American Ceramic Society*, 81(6), pp.1453-1460.
- [53] Lee, S.G., Kim, Y.W. and Mitomo, M., 2001. Relationship between microstructure and fracture toughness of toughened silicon carbide ceramics. *Journal of the American Ceramic Society*, 84(6), pp.1347-1353.
- [54] Moradkhani, A., Baharvandi, H., Tajdari, M., Latifi, H. and Martikainen, J., 2013. Determination of fracture toughness using the area of micro-crack tracks left in brittle materials by Vickers indentation test. *Journal of Advanced Ceramics*, 2(1), pp.87-102.
- [55] Kozekanan, B.S., Moradkhani, A., Baharvandi, H. and Ehsani, N., 2021. Mechanical properties of SiC-C-B<sub>4</sub>C composites with different carbon additives produced by pressureless sintering. *International Journal of Applied Ceramic Technology*, 18(3), pp.957-971.
- [56] Moradkhani, A., Baharvandi, H. and Naserifar, A., 2019. Fracture toughness of 3Y-TZP dental ceramics by using vickers indentation fracture and SELNB methods. *Journal of the Korean Ceramic Society*, 56(1), pp.37-48.
- [57] Najafi, A., Golestani-Fard, F., Rezaie, H.R. and Saeb, S.P., 2021. Sol-Gel synthesis and characterization of SiC-B<sub>4</sub>C nano powder. *Ceramics International*, 47(5), pp.6376-6387.
- [58] Najafi, A., Golestani-Fard, F., Rezaie, H.R. and Ehsani, N., 2011. Synthesis and characterization of silicon carbide nano powder by sol-gel processing. *Iranian Journal of Materials Science and Engineering*, 8(2), pp.41-47.
- [59] Najafi, A., Golestani-Fard, F. and Rezaie, H.R., 2018. Sol-gel synthesis and characterization of B<sub>4</sub>C nanopowder. *Ceramics International*, 44(17), pp.21386-21394.
- [60] Kozekanan, B.S., Moradkhani, A., Baharvandi, H. and Ehsani, N., 2022. Thermodynamic and phase analysis of SiC-nano/microB<sub>4</sub>C-C composites produced by pressureless sintering method. *Journal of the Korean Ceramic Society*, 59(2), pp.180-192.